Photoreactivity of Thiophene-Based Core@Shell Nanoparticles: The Effect of Photoinduced Charge Separation on In Vivo ROS Production

Photoreactivity of thiophene-based core@shell nanoparticles: The Effect of Photoinduced Charge Separation on in vivo ROS Production

Mattia Zangoli[§‡], Andrea Cantelli[Ø‡], Andrea Candini[§*], Anna Lewinska[ǂ], Federica Fardella[Δ], Angela Tino[Δ], Giuseppina Tommasini[Δ], Maciej Wnuk[ǂ], Matteo Moschetta[¶], Sara Perotto[¶], Marco Lucarini[Ø], Claudia Tortiglione[Δ], Guglielmo Lanzani[¶], Francesca Di Maria[§*]

[§] *Istituto per la Sintesi Organica e Fotoreattività (ISOF), Consiglio Nazionale delle Ricerche, Via Gobetti 101, I-40129 Bologna, Italy*

[Ø] *Dpt of Chemistry Giacomo Ciamician, University of Bologna, Via Selmi 2, I-40126 Bologna, Italy*

[Δ] *Istituto di Scienze Applicate e Sistemi Intelligenti "E. Caianiello", Consiglio Nazionale delle Ricerche, Via Campi Flegrei 34, I-80078 Pozzuoli, Italy*

[ǂ] *Department of Biotechnology, University of Rzeszow, Pigonia 1, 35-310 Rzeszow, Poland*

[¶] *Center for Nano Science and Technology @PoliMi, Istituto Italiano di Tecnologia,via Pascoli 70/3, 20133 Milano, Italy.*

KEYWORDS. Organic core-shell nanoparticles, photoinduced charge separation, photoreactivity, Kelvin Probe force microscopy, electron paramagnetic resonance, *in vitro* and *in vivo* ROS generation.

ABSTRACT

Here, we show that in thiophene-based core@shell nanoparticles, namely, P3HT@PTDO NPs, the nanosegregation of the materials results in a peculiar photoreactivity, which, together with their soft and biocompatible nature, makes them interesting bioplatforms. By combining macroscopic and microscopic Kelvin probe measurements, we show that the surface of core@shell NPs becomes rich in negative charges under light illumination─due to the promotion of photogenerated electrons from the inner P3HT core to the outer oxidized PTDO shell─making them more reactive to the environment (air dopants, water, substrate, etc.). Fluorometric and electron paramagnetic resonance (EPR) techniques revealed the formation of transient reactive oxygen species (ROS) upon illumination of aqueous suspensions of NPs, indicating their photoredox reactivity. Detailed analysis permitted to reveal a type I mechanism in ROS generation, ruling out the formation of potentially biodamaging singlet oxygen species. Finally, the biocompatibility of these systems was tested in cells and Hydra polyps. Core@shell NPs exhibit perfect viability and allow the modulation of ROS generation depending on the shell's oxygenation degree, both in vitro and in vivo, in agreement with EPR measurements.

1. Introduction

In recent years, organic nanomaterials have attracted increasing attention for their possible implementation as *soft* biointerfaces in a wide range of applications spanning from implantable biodevices, to sensors, theranostic agents and bioactuators.[1-3] Nowadays, research in this field aims at achieving a deeper understanding of the fundamental interactions between organic materials and biological entities in order to engineer more effective and controlled bioresponses.[4-6]

Among the different classes of nanomaterials, semiconductive thiophene-based nanoparticles (NPs) present numerous advantages for bioapplications because of their synthetic versatility and straightforward functionalization, tunable opto-electronic properties, photoresponsiveness, and

negligible toxicity.[7-10] In particular, these materials have recently emerged as effective *biotransducers* for their capability of converting a light input into an electrical/chemical signal, which in turn can act as a stimulus to live cells with a high temporal and spatial resolution.[11] It has been shown that poly(3-hexylthiophene) NPs (P3HT NPs) are able to operate as biocompatible light-activated interfaces stimulating retinal neurons and recovering visual functions in a rat model of retinis pigmentosa.[12,13] Furthermore, when P3HT-NPs are internalized into the tissue of the small invertebrate model *Hydra Vulgaris*, which lacks eyes but can respond to light stimulation, they induce a modulation of the animal's photobehaviour demonstrating their bioactivity also in not-excitable backgrounds.[14] Nevertheless, the phototransduction mechanism leading to cellular stimulation is still unclear, as more than one phenomenon can be involved in the conversion of light into a cell's physiological output. The most accepted mechanisms are either i) *electrical* due to the capacitive coupling induced by electronic charges accumulated at the surface of the active material, or ii) *photo-electro chemical* due to redox reactions occurring at the NP surface, or iii) a combination of the two.[11,15-19]

Primary photoexcitation of P3HT NPs does not lead to the generation of separated charge carriers. However, in the biological environment, the presence of aqueous medium, together with oxygen-induced photoactivated doping, can promote photoredox reactions able to polarize the outer layer of NPs.[19-23] Light irradiation, in this case, has the main effect of accelerating the polarization process at the NP's surface. Furthermore, the rather long lifetimes of these charged states, up to ms, can favor photocatalytic activities at the interface with electrolytes present in the extracellular environment.[20-23] In favor of this, it has been shown that both in human and *Hydra* cells, light irradiation of internalized P3HT NPs induces a variation of the intracellular production of reactive oxygen species (ROS) depending on NPs concentration.[23]

Recently, we reported that the surface of P3HT NPs can be chemically post-functionalized by oxidizing the outer polymer chains resulting in core@shell NPs (P3HT@PTDO NPs).[24] In these systems, the spatial segregation between the core and shell materials in combination with their different electron affinity, E_{ea}PTDO > E_{ea}P3HT, is expected to efficiently promote photoinduced energy and charge transfer processes from the core to the shell.

To better understand the phototransduction mechanism operating in these innovative nanosystems, we first investigated the photogeneration of charges under illumination through different microscopic and macroscopic techniques and then studied aqueous photochemical reactions occurring at the surface.

Here we show that the combination of Kelvin Probe Force Microscopy (KPFM) and macroscopic Kelvin Probe (KP) techniques enable to observe and characterize the transfer of photogenerated electrons from the inner P3HT core to the outer oxidized PTDO shell. Fluorometric and electron paramagnetic resonance (EPR) techniques show that the increased photoinduced charge separation caused by the core@shell nanoarchitectures enhances the generation of ROS in water suspensions. Furthermore, EPR experiments shed light on the mechanism involved in their generation by excluding a type-II photochemical pathway, (*i.e.*, excluding the formation of $^1O_2$, which is considered the predominant primary ROS involved in photodynamic therapy).

To evaluate how these photophysical characteristics of core@shell NPs influence phototransduction processes occurring at the biotic/abiotic interface of biological systems, differently oxidized core@shell NPs were administered to HEK-293T cells and Hydra polyps (*i.e.*, simple freshwater invertebrates employed as *in vivo* model systems). *In vivo* photoexcitation of NPs not only does not cause toxicity in biological systems, but also determines a variation of the

intracellular redox balance which is finely modulated/regulated by the degree of oxygenation of the shell.

Looking ahead, this work shows a new route to chemically tailor the photogeneration of ROS in organic core@shell nanoarchitectures, thus opening the way for the development of new photoactive transducers for precise ROS optical modulation *in vivo*, at non-toxic levels, aimed at therapeutic purposes.[25]

2. Synthesis and surface photovoltage characterization of core@shell NPs

Different batches of P3HT@PTDO$_x$ NPs were prepared by directly oxidizing water suspensions of P3HT NPs with x = 0.5, 1.0, and 1.5 equivalents of HOF·CH_3CN, according to reference 23 (see Figure S1). The addition of up to 1.5 equivalents of HOF·CH_3CN does not perturb the physical stability of the suspension. Conversely, the insertion of a larger number of TDO units on the NPs shell results in a progressive increase of the zeta potential value, which is indicative of a rise in the electrostatic repulsion between particles, while their sizes remain approximately constant (see Table S1). The morphology and surface potential (SP) characteristics of the NPs were investigated by Atomic Force Microscopy (AFM) and Kelvin Probe Force Microscopy (KPFM), a contactless technique that allows the non-invasive quantitative mapping of electronic surface properties of nanostructures.[26-27] KPFM measurements were performed in dark and after illumination to investigate the possible effects of charge generation at the core/shell interface. Figure 1 shows the morphological and SP images of P3HT@PTDO$_{1.5}$ NPs. To a first approximation, SP can be directly related to the work function of the sample, being the difference between the work function of the tip and the material (SP = $\left|WF_{tip}\right| - \left|WF_{sample}\right|$).

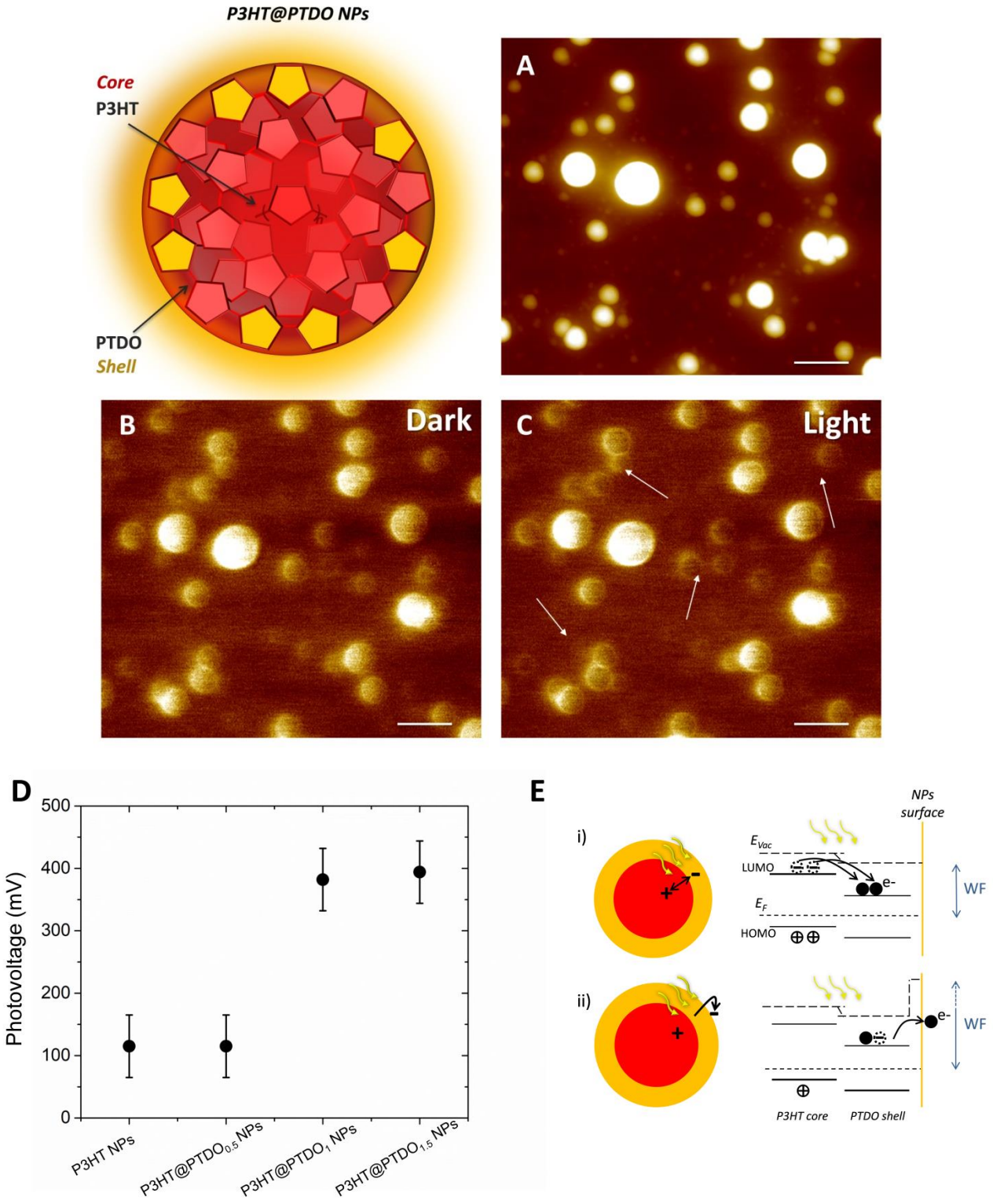

Figure 1. Top: schematic illustration of the core@shell NPs. A) Topography image of the P3HT@PTDO$_{1.5}$ NPs on Si substrate. B,C) Corresponding surface potential images were taken in dark and after 4h of irradiation with a white halogen lamp of intensity < 0.6 mW/mm^2. Scale bars: 1 μm; z-range: (A) 160 nm; (B-C) 40 mV. D) Photovoltage versus the oxidation degree of the

P3HT NPs. Positive values indicate a loss of photogenerated electrons. E) Schematic representation of the proposed mechanism: i) photogenerated electron-hole pairs are separated with the negative charges being kept at the PTDO shell; ii) upon continuous light excitation, additional electrons at the PTDO are further excited and trapped by surface states.

P3HT@$PTDO_{1.5}$ NPs, whose diameter is in the range of ~ 200 nm (Figure 1A), present an outer corona, *i.e.*, a shell made of oxygenated polymer (PTDO), which is characterized by SP values higher than the inner part, *i.e.*, the core constituted by pristine P3HT (Figure 1B-C). This implies that at the shell the Fermi energy is closer to the vacuum, analogously to an electron doping of the material. As shown in Figure 1B-C, this feature is observed both in the dark and after illumination and is consistent with the greater electron affinity of the PTDO polymeric chains[28] present on the shell of the NPs compared to pristine P3HT NPs. Furthermore, after light excitation, the overall surface potential decreases and several NPs (some marked with arrows in Figure 1C) show an enhancement of the contrast between the inner and outer parts. Accordingly, Figure S2, which reports the difference between images 1B and 1C, *i.e.*, (dark – light), shows that for most of the NPs the outer corona disappears or displays a dark contrast, indicating that under the illumination the SP value of the shell is decreased less than that of the core, *i.e.*, the above mentioned electron-doped character of the shell versus the core is further enhanced. These observations suggest the presence of a significant electron transfer from the core to the shell of the NPs, thus corroborating the presence of photoinduced charge separation at the interface.

P3HT@PTDO NPs were also investigated with macroscopic Kelvin Probe (KP) to study photoinduced charge generation.[27,29] The technique employs a tip with a diameter of ~2 mm, thus averaging over a large number of NPs (which at these length scales can be considered as a uniform film) and, consequently, being the film thicker than the subsurface sensitivity the measurement is not affected by the contribution from the substrate. Figure 1D depicts the dependence of the surface

photovoltage (SPV, *i.e.*, $SP_{dark} - SP_{light}$) versus the NPs oxidation degree. Positive SPV values are found for all NPs ─ that is, a lowering of the SP after the illumination (which in our experimental setup means an increase of the measured work function) ─ in agreement with KPFM characterizations. Furthermore, the SPV is significantly higher for core@shell NPs with a high degree of oxidation (P3HT NPs ≈ P3HT@$PTDO_{0.5}$ NPs < P3HT@$PTDO_1$ NPs ≤ P3HT@$PTDO_{1.5}$ NPs).

Based on our experimental results, we propose that, upon light absorption, electron-hole pairs are generated and a sizeable fraction of the free electrons are captured by the electron acceptor units, *i.e.*, thiophene-S,S-dioxide, of the PTDO present in the shell of the NPs (Figure 1Ei). During the long exposure times (4h), these additional electrons are likely to be further excited and trapped by surface states, with the final effect that the shell becomes rich in negative charges, thus increasing the measured work function (Figure 1Eii). Nevertheless, the additional contribution of possible photoreactions cannot be excluded *a priori.* In this regard, we can conclude that core@shell nanostructures, in the presence of light, present a superior ability to accumulate electrons on the NPs surface than pristine P3HT NPs and this effect is amplified when the thickness of the oxidized shell increases. These loosely bounded charges at the surface of nanomaterials could be more available to react with the environment (air dopants, water, substrate *etc*.) prompting us to evaluate the possible ROS production under illumination.

3. Determination of ROS species in core@shell NPs

To assess the photoredox activity of core@shell NPs, in particular, the formation of ROS species in physiological environments, fluorometric and electron paramagnetic resonance (EPR) techniques were employed.[30] Accordingly, measurements were performed in PBS 50 mM at pH 7.4 to mimic the ionic strength and pH of the physiological environment.

It is known that, upon light activation, a photosensitizer can undergo type I and/or type II reactions resulting in the formation of ROS species, such as singlet oxygen ($^1O_2$), superoxide radical anion ($\cdot O_2^-$), hydroxyl radical ($\cdot$OH), hydrogen peroxide (H_2O_2).[31-34] Firstly, the possible occurrence of the type II photodynamic mechanism ─ which involves the photosensitized generation of $^1O_2$ through a direct energy transfer between the photosensitizer excited triplet state and molecular oxygen (O_2) ─ was investigated in all NPs samples by means of EPR measurements.[32-35] The formation of $^1O_2$ upon light irradiation was checked using 4-oxo-2,2,6,6-tetramethylpiperidine (4-oxo-TEMP), a well-known water-soluble probe.[36] 4-oxo-TEMP reacts with $^1O_2$ forming a stable paramagnetic species, *i.e.*, 4-oxo-TEMPO, characterized by easily recognizable EPR spectral features.[37,38] It was found that $^1O_2$ is not formed neither in P3HT-NPs nor in core@shell NPs samples; indeed, no EPR signals diagnostic of the formation of 4-oxo-TEMPO, were detected, thus ruling out ROS generation via a type II mechanism. This finding suggests that faster triplet state quenching mechanisms are active in these systems. Subsequently, the involvement of a type I mechanism in ROS production was investigated by EPR and fluorometric techniques. While the former allows detection of transient free radicals generated by electron transfer processes, *i.e.*, $\cdot O_2^-$ and $\cdot$OH, the latter reveals peroxides accumulated in solution. 5,5-dimethylpyrroline-*N*-oxide (DMPO) was employed as a spin trap probe in EPR measurements because of its ability to intercept and react with $\cdot O_2^-$ and $\cdot$OH, generating the respective adducts DMPO-OOH and DMPO-OH characterized by longer lifetimes and distinct EPR signals. As shown in Figure 2, spin trap experiments revealed that all NPs generate significant amounts of either $\cdot$OH or $\cdot O_2^-$ transient free radicals, confirming ROS generation through the type I mechanism. The EPR spectra of all samples consist of two components, in particular, signals with a_N = 14.2 G, a_H^{β} = 11.4 G and $a_H^{\gamma 1}$ = 1.2 G indicative of a DMPO-OOH adduct, and signals with $a_N = a_H$ = 14.75 G characteristic of

a DMPO-OH adduct. Both adducts were observed simultaneously at the beginning of the irradiation process. Furthermore, the fact that significant conversion of DMPO-OOH into DMPO-OH was not observed suggests that both radical species are produced upon irradiation of the photosensitizers. The different contribution deriving from the two species was assessed by *i*) delaying the spectral acquisition after irradiation, to let the DMPO-OOH signal decay and leave the DMPO-OH signal alone because of its longer lifetime; *ii*) performing the measure in the presence of 8% v/v DMSO, to quench the ·OH radical thus leading to the preferential accumulation of DMPO-OOH generated by $\cdot O_2^-$(see Figure S3).[36]

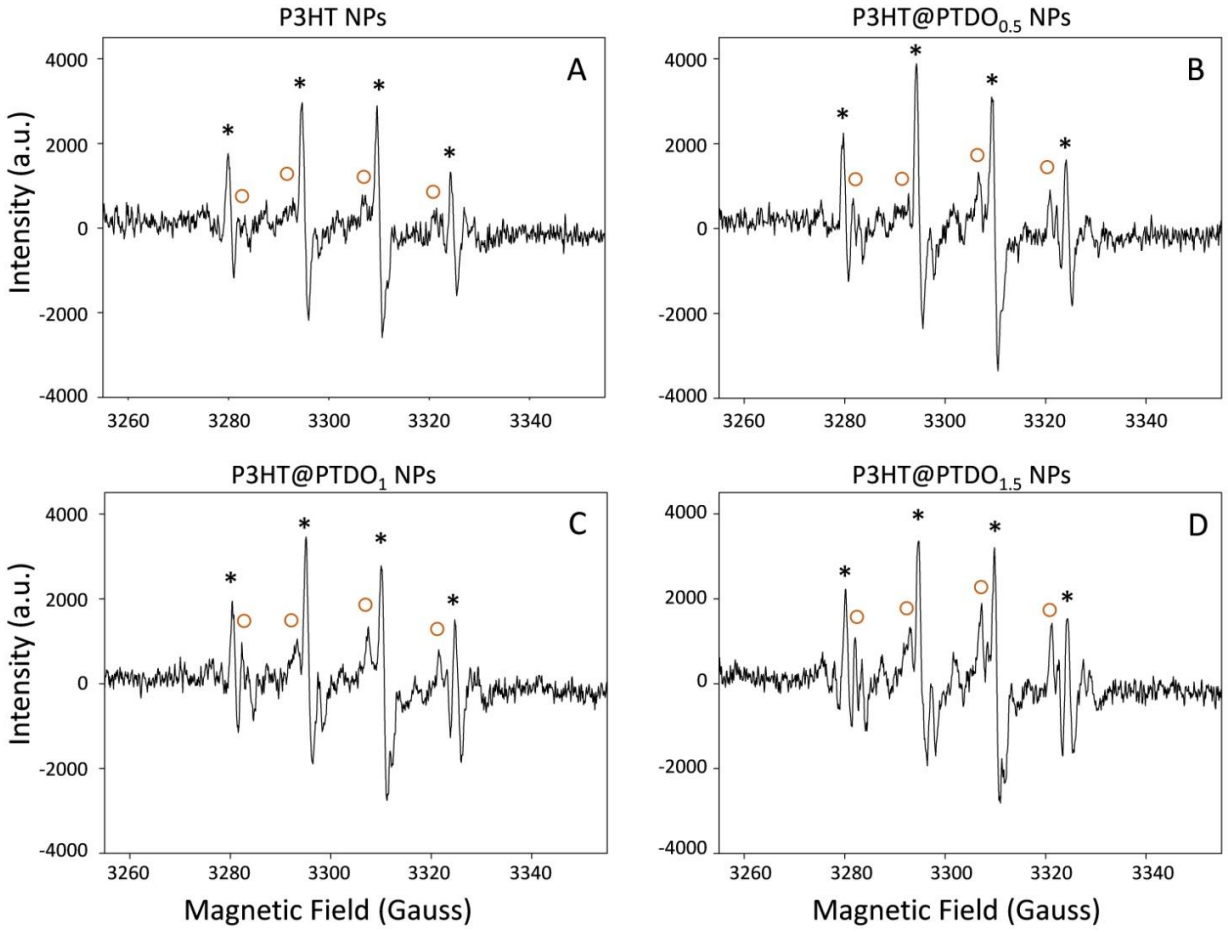

Figure 2. EPR spectra of P3HT NPs (A) and core@shell NPs (B: P3HT@PTDO$_{0.5}$ NPs; C: P3HT@PTDO$_1$ NPs; D: P3HT@PTDO$_{1.5}$ NPs), under irradiation, in the presence of DMPO (* DMPO-OH, ○ DMPO-OOH).

It is important to note that many photosensitizers require the presence of an electron/proton donor to undergo the type I mechanism for ROS generation and, for this reason, additional reagents (*e.g.* NADH) are often added in solution during measurements to simulate the redox active conditions of physiological environments.[36] Noteworthy, in these systems, type I mechanism ROS generation is triggered without the use of additional redox-active substances, indicating that NPs can accomplish this function on their own.

Finally, the presence of peroxides, such as H_2O_2, ROOH, produced upon irradiation, was assessed using an Amplex Red fluorimetric assay. As shown in Figure 3, after 4 h under white light irradiation, all NPs samples produced significant concentrations of peroxides above the micromolar unit, further confirming an active type I mechanism for ROS generation. The main peroxide detected after irradiation is most likely H_2O_2 derived from the dismutation of the $\cdot O_2^-$,[33] although a concomitant formation of organic peroxides, such as ROOH, *via* more complex pathways, cannot be completely ruled out.

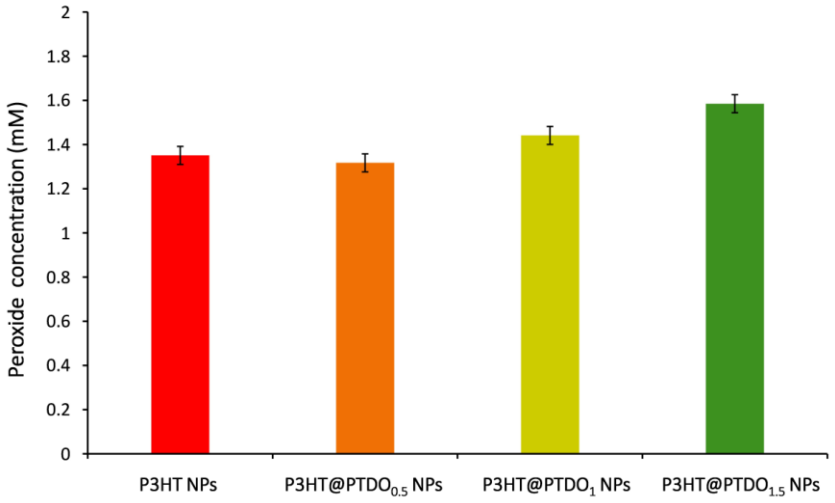

Figure 3. Generation of peroxides during visible light irradiation of P3HT NPs and P3HT@PTDO$_x$ NPs samples.

EPR and fluorometric experiments revealed that core@shell NPs are able to produce more radical species than pristine P3HT NPs, and the amount is proportional to the oxidation degree of the NPs shell (Figures 2,3). Considering that an electron transfer is required for ROS generation,[35,36] the fact that P3HT@PTDO$_x$ NPs are more effective than P3HT NPs can be rationalized by taking into account their greater tendency to donate electrons from their surface, as demonstrated by KPFM measurements. Furthermore, the dependence of ROS production on the shell's oxidation degree is probably related to the progressive increase of electron affinity of the outer polymer chains which favor the electron transfer process.

4. Core@shell NPs in living cells and *Hydra* polyps

To assess the biocompatibility of these systems, P3HT NPs and P3HT@PTDO$_x$ NPs (x= 0.5, 1, 1.5) were administered both in living HEK-293T cells and Hydra polyps.

In HEK-293T cells, regardless of the degree of oxidation of the shell, all NPs 24 h after the exposure: i) internalize into the cell without causing evident disruption of the plasma membrane, ii) localize at the level of the cytoplasm, and iii) have no cytotoxic effect, neither in dark nor in light conditions (670 μW/mm^2 in continuous for 5 minutes), as evidenced by AlamarBlue assay (Figures 4E and S4).

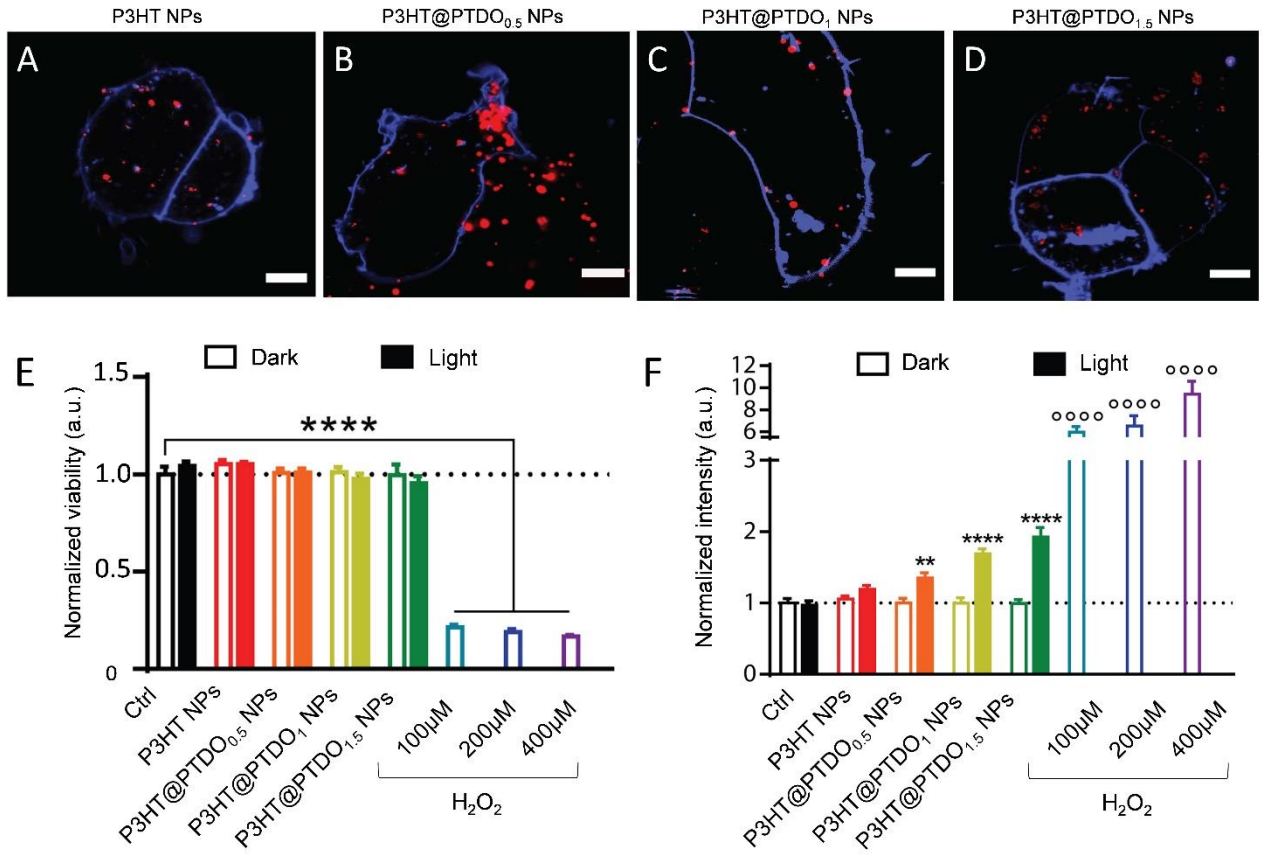

Figure 4. A-D) Representative confocal images of NPs loaded in HEK-293T cells and their localization within the cytoplasm 24 hours after the incubation. In blue CellBright that marks the plasma membrane and in red NPs. Scale bars, 5μm. E) Histograms showing cell viability evaluated 24 h after treatment with NPs. Data are represented as means ± sem. Two-way ANOVA with Bonferroni's correction and one-way ANOVA with Dunn's test correction (n=9 for NPs treated samples and n=6 for samples treated with H_2O_2; ****$p < 0.0001$). F) Histograms showing ROS level evaluated 24 h after treatment with NPs. Data are represented as means ± sem. Two-way ANOVA with Bonferroni's correction and Kruscal-Wallis with Dunn's test correction (n=16-23 fields for each experimental group; **$p<0.01$; ****$p<0.0001$ between dark and light conditions; °°°°$p<0.0001$ when compared to Ctrl dark condition).

To evaluate the intracellular effect induced by the photostimulation of NPs (that is, the effects of charge generation at the core/shell interface), we measured ROS production within the cytosol of HEK-293T cells treated with NPs with different oxidation degree, either in dark or under illumination. 2,7-dichlorodihydrofluorescein diacetate (DCFDA) was employed as a cell-permeant probe to assess ROS formation before and after light stimulation.[39] As shown in figure 4F, under

dark conditions, cells treated with differently oxidized core@shell NPs show the same behavior as untreated cells with no significant increase in ROS production. Otherwise, under illumination, a progressive increase in ROS production as a function of the shell's oxygenation level of the NPs is observed: the greater the oxidation of the shell, the greater the amount of ROS generated. Nonetheless, even at the higher shell's oxygenation level of the NPs, the amount of ROS is never greater than 2-fold the one detected in control cells. To verify if the amount of generated ROS is potentially harmful to the biological matter, cells were exposed to toxic concentrations of H_2O_2 (100-400 μM).[40] As shown in figure 4E, the potential level of H_2O_2 produced by core@shell NPs is well below the threshold values that cause oxidative stress and subsequent cell death, as previously underlined in the viability assay (Figure 3E).[40] It is reasonable to hypothesize that, after the end of the illumination protocol, ROS are slightly reduced in concentration due to the action of enzymes capable of eliminating oxygen species (such as catalyze, peroxidase and superoxide dismutase) which contribute to the maintenance of cell healthiness.

In *Hydra* tissue, the degree of internalization of NPs was confirmed by confocal and optical microscopy. *Hydra* presents simple structural anatomy, resembling a hollow tube with a foot to anchor to a substrate and a single mouth opening at the oral end surrounded by a tentacle crown. The transparency of its body tissue allows visualizing the internalization of any fluorescent compound added to the medium.[41] As shown in Figures 4 and S5, NPs are evenly distributed throughout the body, from tentacles to the foot regions, although the granular pattern of fluorescence on the body column seems to progressively decrease as the degree of oxidation of the shell increases (Figure S5).

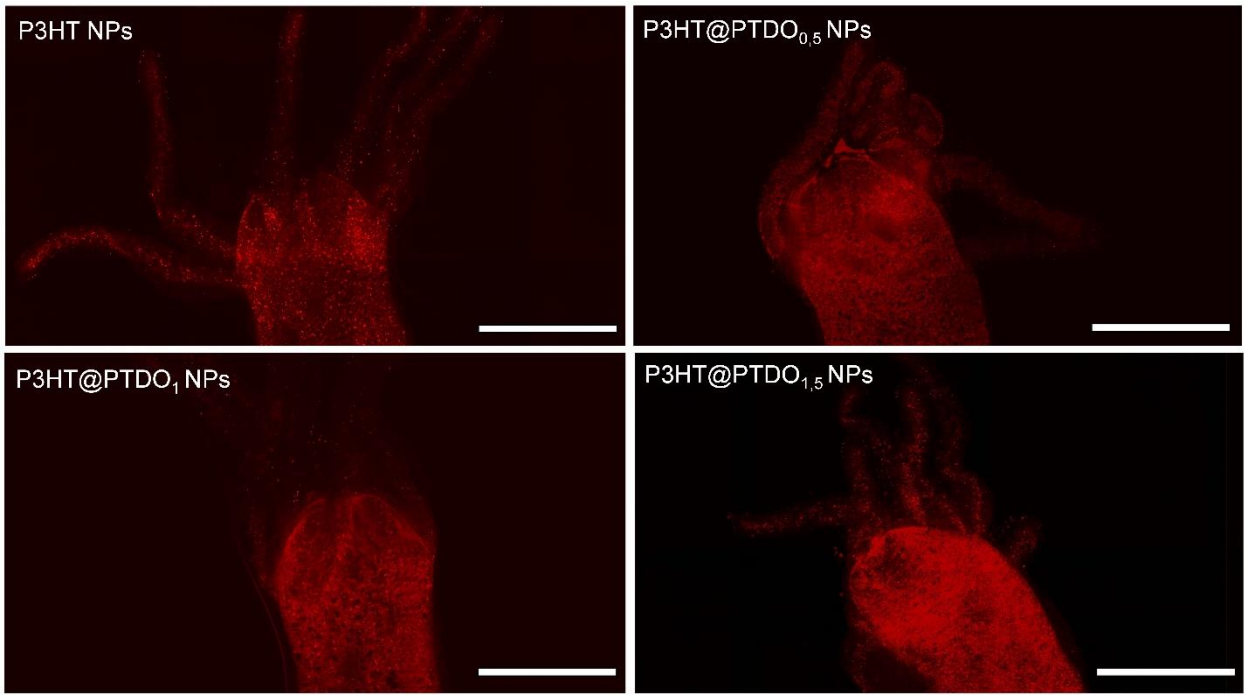

Figure 4. Biodistribution of P3HT NPs (A) and P3HT@PTDO$_x$ NPs (B-D) in Hydra tissue by confocal imaging. Scale bars, 500 μm.

The biocompatibility of core@shell NPs was determined using a well-established morphometric test based on visible alterations in the polyps, *i.e.* body contraction, cell loss, and tentacle disintegration, possibly induced by the exposure to toxicants.[42,43] Dose-response assays were performed by adding P3HT@PTDO$_x$ NPs in increasing doses (from 25 to 100 μg/ml) to a group of 20 polyps and incubating up to 72 h. As shown in Figure S6, none of the NPs was found to have toxic effects up to the highest dose tested (100 μg/ml) which was then used for further analysis.

It is known that ROS can directly trigger the oxidation of macromolecules within the cell resulting in a variety of damaged sites.[44] To assess the effect induced by photostimulation of core@shell NPs in Hydra, we evaluated the extent of DNA oxidative damage by measuring the levels of 8-hydroxy-2′-deoxyguanosine (8-OHdG), *i.e.*, a product of oxidatively DNA damage formed by hydroxyl radical, singlet oxygen, and the levels of 5-hmC, *i.e.*, the first oxidative product in the active demethylation of 5-methylcytosine (5mC), found deregulated in stress condition.[45,46] Polyps

were treated with P3HT NPs, P3HT@$PTDO_1$ NPs and P3HT@$PTDO_{1.5}$ NPs, and exposed to the white illumination of a led source (0.124 mW/mm^2) for 4 h and 24 h before DNA extraction and processing. Figure 5 shows that the photostimulation of NPs affects the expression of both 8-OHdG and 5-hmC. Indeed, their levels gradually rise as the shell oxidation increases (P3HT NPs < P3HT@$PTDO_1$ NPs < P3HT@$PTDO_{1.5}$ NPs), both at 4 h and 24 h, thus supporting the increased ROS generation by the most oxidized NPs (Figure 5A-B). It is important to note that, after 4 h illumination, 5-hmC levels are significantly upregulated in samples treated with core@shell NPs compared to P3HT NPs (Figure 5C). After 24 h this effect is less evident, however, modulation of 5-hmC levels is observed also in dark conditions, thus indicating a biochemical effect of these NPs even in the absence of light illumination (Figure 5D).

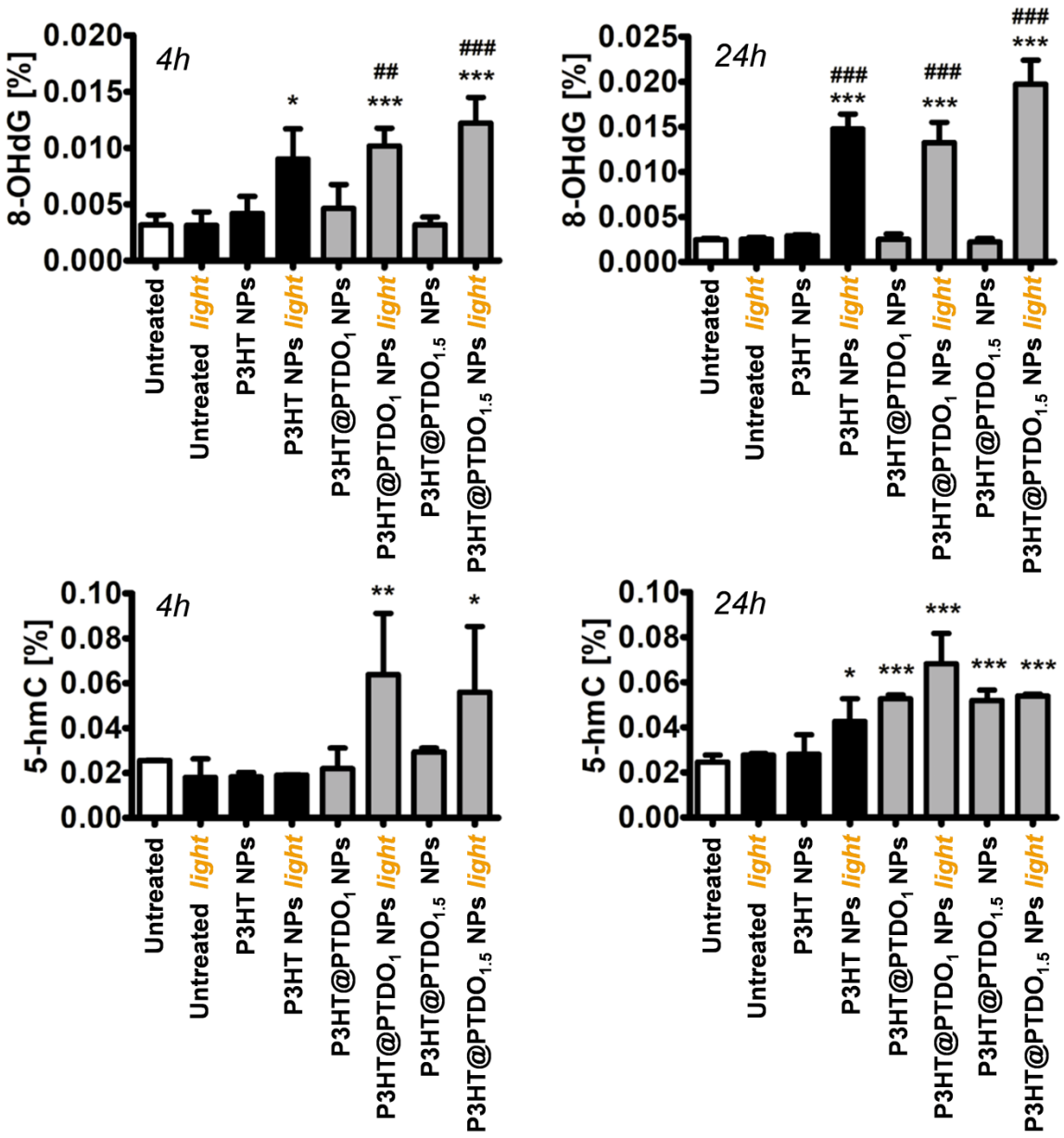

Figure 5. The effect of photostimulation of P3HT or P3HT@PTDO$_x$ NPs on the levels of 8-OHdG (upper panel) and 5-hmC (down panel) in *Hydra* DNA. *Hydra* polyps were exposed to the white illumination of a led source for 4 h (left panel) and 24 h (right panel). The results were presented as %. Bars indicate SD, n > 4, $^{***}p < 0.001$, $^{**}p < 0.01$, $^{*}p < 0.05$ compared to untreated animals (ANOVA and Dunnett's a posteriori test). Two-tailed paired Student's t-test was also used to compare animals treated with P3HT- or P3HT@PTDO$_x$ -NPs under dark or light conditions; $^{###}p < 0.001$, $^{##}p < 0.01$.

Despite the significant increase in the level of oxidative stress indicators, the animals do not show any morphological alteration nor a reduction in their viability. These results are consistent and perfectly in line with what was observed in HEK-293T cells confirming that P3HT@PTDO$_x$ NPs are suitable for biological applications.

5. Conclusion

Here we demonstrate experimentally that thiophene-based core@shell NPs are systems capable of separating charges under illumination. This is due to their layered structure composed of two materials with different electron affinities as directly observed by microscopic KPFM measurements. Furthermore, macroscopic Kelvin probe experiments proved that the outer shell of core@shell NPs, when exposed to light, becomes enriched in negative charges thus reaching higher SPV values. The accumulation of photogenerated charges on the NPs surface confers to these systems photoredox characteristics making them prone to participate in unique reaction pathways. EPR and fluorometric techniques confirmed the ability of core@shell NPs to photogenerate ROS species through a type I mechanism that does not entail the formation of harmful singlet oxygen. Finally, we show that core@shell NPs are fully biocompatible, both in living HEK-293T cells and *Hydra* polyps and allow to modulate *in vitro* and *in vivo* ROS levels in a light- and shell oxidation-dependent manner. In conclusion, our measurements pave the way for the utilization of thiophene-based core@shell NPs as exogenous photoactuators which can potentially operate through two different mechanisms based on charge capacitive effects and/or ROS generation inside living organisms.

6. Experimental section

$^1O_2$ detection by EPR method. $^1O_2$ was detected by EPR using 2,2,6,6-tetramethyl-4-piperidone (4-oxo-TEMP, Sigma-Aldrich, cat. no. 459119) as a probe. Measures were performed on water solutions containing: 5% NPs, 4-oxo-TEMP 0.08M, PBS 50mM at a pH of 7.4. Portions of the

sample (10 μL) were irradiated in a glass capillary tube under aerobic conditions. The generation of singlet oxygen was detected by the three lines EPR signals (a_N = 16.13 G) corresponding to 4-oxo-TEMPO, formed by the reaction of $^1O_2$ with 4-oxo-TEMP. Rose Bengal was used as a reference singlet oxygen generating compound.

˙OH detection by EPR spin-trapping method. ˙OH was detected by EPR using 5,5-dimethyl-1-pyrroline-*N*-oxide (DMPO, Sigma-Aldrich, cat. no. 92688) as a spin-trapping reagent. Measures were performed on water solutions containing: 5% NPs, DMPO 8% v/v, PBS 50 mM at pH 7.4. Portions of the sample (10 μL) were irradiated in a glass capillary tube under aerobic conditions. The generation of ˙OH was detected by the four lines signal corresponding to DMPO-OH, formed by the reaction of ˙OH with DMPO.

Detection of Superoxide Radical Anion (EPR Spin-Trapping Method). For the detection of this radical, it has been used 5,5-Dimethyl-1-pyrroline N-oxide (DMPO) as a spin-trap. Measures were performed on water solutions containing: 5% NPs, DMPO 8% v/v, in PBS 50 mM at pH 7.4. Portions of the sample (10 μL) were irradiated in a glass capillary tube under aerobic conditions and no reductants were added to the solution. The generation of ˙OH was detected by the signal corresponding to DMPO-OOH, formed by the reaction of $˙O_2^-$ with DMPO. In the experiments conducted to isolate the EPR signal of DMPO-OOH, 8% v/v DMSO was added to the solvent to quench the ˙OH produced during the irradiation, thus disadvantaging the formation of DMPO-OH.

Amplex Red peroxides detection. The ability to generate peroxides in solution, upon irradiation with visible light, was evaluated using Amplex Red fluorometric assay. Colourless nonfluorescent Amplex Red reacts with peroxides, catalyzed by HRP, to form a coloured and fluorescent resorufin. The concentration of peroxides produced during the irradiation is calculated as the difference of resorufin generated by the irradiated sample solutions and that of their relative references, *i.e.*, identical solutions kept in the dark.10 μL of Amplex Red 50 mM in DMSO was added to 1 ml of phosphate buffer 50 mM pH 7.4. Then 10 μL of HRP 0.4 mg/ml in PBS was added to the Amplex Red solution to obtain the final working solution. 90 μL of the solutions under investigation in PBS 50 mM pH 7.4, were irradiated for 4 h with visible light on 96 well microtiter plates (white LED Valex 30 W lamp at 30 cm distance from plate, irradiation power density on the cell plate = 2.4 mW/cm^2; measured with the photo-radiometer Delta Ohm LP 471 RAD).10 μL of Amplex Red working solution was added to each sample (and to the relative reference kept in the dark) immediately after irradiation. After 30 min of incubation at room temperature, the fluorescence of the samples was read at 590 nm. A calibration curve generated using standard solutions of H_2O_2 was used to convert the fluorescence signal to the concentration of the peroxide generated upon irradiation. Fluorescence measurements were carried out using a Perkin Elmer EnSpire® Multimode Plate Reader.

Cell culture maintenance. *In vitro* experiments were performed using the immortalized cell line HEK-293T (Human Embryonic Kidney), purchased from ATCC. HEK293T cells were cultured in T-25 cell culture flasks containing Dulbecco's Modified Eagle Medium high glucose (DMEM-HG) culture medium, supplemented with 10% heat inactivated Foetal Bovine Serum (FBS) and 1% GlutaMAX (0.5mM, Invitrogen). Culture flasks were maintained in a humidified incubator at 37 °C with 5% CO_2. When at confluence, cells were enzymatically detached from the flasks with a 1x trypsin-EDTA solution, plated on sterilized substrates and left to grow for 48 h before performing the experiments. Prior to cell plating, a layer of fibronectin (2 μg ml^{-1} in PBS buffer solution) was deposited on the sample surface and incubated for 1 h at 37 °C to promote cellular adhesion.

Viability assay. To assess NPs biocompatibility, AlamarBlue proliferation assay was performed. The toxicity assay with AlamarBlue is an indirect method, based on the quantitative measurement of cellular metabolic activity by measuring fluorescence. Resazurin, the active principle in the AlamarBlue reagent, is a non-fluorescent and non-toxic compound, permeable to the cell membrane. Viable cells reduce resazurin to resofurin, a highly fluorescent compound. The conversion from the oxidized to the reduced form causes an absorption shift from 600nm to 570nm. For this experiment, 4000 cells/cm^2 were plated 48h before the experiment. 24h after plating, samples were incubated with NPs (5% w/w) at 37 °C, in a humidified 5% CO_2 atmosphere. After 24h of incubation, half of the samples were exposed to light (530 nm, 670 μW/mm^2, 5 minutes). The AlamarBlue Reagent (Invitrogen DAL 1100) was diluted 1:10 with DMEM without phenol red. The solution without the cell was used as blank. The samples were incubated for 4 hours and subsequently, a 100μl aliquot of the solution was removed from each well and transferred to a 96-well plate. The fluorescence was detected using a fluorescence spectrophotometer, exciting at 560 nm and measuring the emission at 590 nm. The emission value was acquired 3 times per aliquot to obtain a reliable measure.

Localization experiments. 6000 cells/cm^2 were plated 48h before the experiment. After 24h cells were incubated with NPs (5% w/w) and maintained in an incubator. 24 h after incubation, samples were washed with PBS to remove NPs that were not internalized. Next, samples were incubated for 40 minutes with CellBright™ Blue Cytoplasmic Membrane-Labeling Kit (10μl/ml; Biotium) to detect cell plasma membrane. Samples were washed with PBS to remove cell unbound molecules, and the acquisition was performed using 60X objective. 403.3 nm and 561 nm lasers were used to excite CellBright and NPs, respectively. The acquired images were analyzed with ImageJ, using the JACoP plugin

ROS detection in HEK293T cells. Cells were plated on glass coverslips for 48h before performing the experiment. Cells were seeded at a density of 6000 cells/cm^2 in a complete culture medium. 24 h after seeding, the cells were incubated with NPs (5% w/w). After 24h of incubation, half of the samples were exposed to light (530 nm, 670 μW/mm^2, 5 minutes). Cells were then stained with 1 μM DCFDA dye (Sigma-Aldrich), diluted in extracellular solution (5 mM HEPES, 135 mM NaCl, 5.4 mM KCl, 1 mM $MgCl_2$, 1.8 mM $CaCl_2$, 10 mM glucose, all purchased from Sigma-Aldrich; pH 7.4). Acquisitions were carried out in the same extracellular solution, with an Olympus BX53 biological microscope, equipped with a solid-state LED stimulation system (Spectra III, Lumencor); a FITC-filtering system (Thorlabs) was used to record only the emission wavelength of the probe. Images were recorded with MetaMorph 7.10.3.288.

Animal culture, toxicological assays. *Hydra Vulgaris* were asexually cultured in *Hydra* medium (1 mM $CaCl_2$ and 0.1 mM $NaHCO_3$, pH 7), according to the method of Loomis and Lenhoof.[47] Polyps were fed three times per week with freshly hatched *Artemia salina* nauplii and kept at 18 ±1 °C with a 12:12 h light: dark regime. For toxicological evaluation, a morphometric assay was performed, assigning numerical scores to precise morphological alterations. Dose-response curves were determined in the range of 25-100 mg/ml in chronic conditions from 24 h up to 72 h.

Imaging of *Hydrae*. Imaging was performed by fluorescence microscopy on living animals treated for 24 h with NPs and relaxed for 2 min in 2% urethane. Images were acquired *in vivo* by a stereomicroscope (Olympus ZSX-RFL2) equipped with fluorescence filter sets (BP460–490/DM505/LP510). Moreover, animals were fixed in 4% paraformaldehyde pH 7.4, at 4°C, rinsed three times in phosphate saline buffers (PBS: 8 g/l NaCl; 0.2 g/l KCl; 1.44 g/l $Na_2HPO_4•7H_20$; 0.24 g/l KH_2PO_4) and mounted on slides with glycerol/PBS before confocal imaging.

Photostimulation. Groups of 20 polyps starved for 24 h were selected from a homogeneous population and treated with NPs in a plastic multiwell in a final volume of 300 ml, at the desired dose and time. Untreated polyps soaked in *Hydra* medium were used as controls. After extensive washing, photostimulation was accomplished by exposing animals to a light emitting diode (LED) white light source (Edmund Optics, the power density of 0,124 mW/mm^2) for 4 h or 24 h. The experimental conditions to estimate the effect of the photostimulation were untreated, NPs/treated, untreated/illuminated, NPs-treated/illuminated.

ELISA 5-Hydroxymethylcytosine (5-hmC) and 8-hydroxy-2-deoxyguanosine (8-OHdG) were measured using MethylFlash Global DNA 5-Hydroxymethylation (5-hmC) ELISA Easy Kit (Colorimetric) and EpiQuik 8-OHdG DNA Damage Quantification Direct Fluorometric Kit, respectively (Epigentek, Farmingdale, NY, USA, P-1032 and P-6004). DNA isolation and analysis were performed according to our previous described protocol.[48] The results represent the mean ± SD from at least two independent experiments and at least 4 technical repeats. Results are presented as %. Statistical significance was evaluated using GraphPad Prism 5. *P*-values of less than 0.05 were considered significant.

DNA oxidation. Oxidative DNA damage, namely the levels of 8-hydroxy-2′-deoxyguanosine (8-OHdG) were measured using Epigentek EpiQuik 8-OHdG DNA Damage Quantification Direct Fluorometric Kit according to the manufacturer's instructions. Briefly, DNA was extracted from 20 *Hydra* in each experimental condition (200 ng) and subjected to 8-OHdG content analysis, as previously reported.[49]

Levels of 5-hydroxymethylcytosine. 5-Hydroxymethylcytosine (5-hmC) was measured using MethylFlash Global DNA 5-Hydroxymethylation ELISA Easy Colorimetric Kit according to the manufacturer's instructions. Briefly, DNA was extracted from 20 *Hydra* in each experimental condition (40 ng) and subjected to 5-hmC content analysis. Absorbance was read at 450 nm using a Tecan Infinite® M200 absorbance mode microplate reader. The calculation was made based on absolute quantification with a standard curve and linear regression function and 5-hmC content in total DNA is presented as %. The results represent the mean ± SD from at least two independent experiments and three technical replicates. Differences between untreated and treated animals were revealed using one-way ANOVA and Dunnett's multiple comparison test. Two-tailed paired Student's *t*-test was also used to compare NPs treated animals versus NP/light treated animals. Statistical significance was evaluated using GraphPad Prism 5. *p*-values of less than 0.05 were considered significant.

ASSOCIATED CONTENT

Supporting Information. Instruments characteristics; Preparation and DLS characterizations of P3HT@$PTDO_x$ NPs; KPFM and EPR measurements; Co-localization analysis of P3HT@$PTDO_x$ NPs in HEK-293T cells; Fluorescence imaging of living *Hydra* polyps treated with of P3HT@$PTDO_x$ NPs. Toxicological evaluation of P3HT@$PTDO_x$ NPs on Hydra.

AUTHOR INFORMATION

Corresponding Author

Dr. Andrea Candini – Istituto per la Sintesi Organica e la Fotoreattività (ISOF) , Consiglio Nazionale delle Ricerche (CNR), Bologna, Italy

Dr. Francesca Di Maria – Istituto per la Sintesi Organica e la Fotoreattività (ISOF) , Consiglio Nazionale delle Ricerche (CNR), Bologna, Italy

Author Contributions

M.Z. and A.C. contributed equally to this work. M.Z. and F.D.M. prepared and characterized P3HT NPs and P3HT@PTDO NPs. A.C. and M.L. performed EPR analysis and analyzed the data. A.C. carried out KP and KPFM measurements. M.M. and S.P. performed experiments on HEK-293 T cells. F.F., A.T., G.T. and C.T., made experiments on Hydra polyps. A.L. and M.W. carried out ELISA tests. C.T. and G.L. discussed and validated the data. A.C. contributed to the writing of the paper. FDM coordinated the project and wrote the paper with inputs from the other authors. All authors have approved the final version of the manuscript.

Notes

The authors declare no competing financial interest.

ACKNOWLEDGMENT

We thank Prof. Shlomo Rozen for helpful and insightfull discussion.

REFERENCES

1) Berggren M., Głowacki E. D., Simon D. T., Stavrinidou E., Tybrandt K. In Vivo Organic Bioelectronics for Neuromodulation. *Chem. Rev*., **2022**, 122, 4, 4826–4846.
2) Fang Y., Meng L., Prominski A., Schaumann E. N., Seebald M., Tian B. Recent advances in bioelectronics chemistry. *Chem. Soc. Rev*., **2020**, 49, 7978-8035.
3) Pitsalidis C., Pappa A. M., Boys A. J., Fu Y., Moysidou C. M., Van Niekerk D., Saez J., Savva A., Iandolo D., Owens R. M. Organic Bioelectronics for In Vitro Systems. *Chem. Rev*., **2022**, 122, 4, 4700–4790.

4) Tang S., Davoudi Z., Wang G., Xu Z., Rehman T., Prominski A., Tian B., Bratlie K. M., Peng H., Wang Q. Soft materials as biological and artificial membranes. *Chem. Soc. Rev*., **2021**, 50, 12679-12701
5) Langer R., Tirrel D. A. Designing materials for biology and medicine. *Nature*, **2004**, 498, 487-492.
6) Li Y., Xiao Y., Liu C. The Horizon of Materiobiology: A Perspective on Material-Guided Cell Behaviors and Tissue Engineering. *Chem. Rev.*, **2017**, 117, 5, 4376–4421.
7) Zangoli M., Di Maria F. Synthesis, characterization, and biological applications of semiconducting polythiophene-based nanoparticles. *VIEW*, **2021**, 2:20200086.
8) Zangoli M., Di Maria F., Zucchetti E., Bossio C., Antognazza M. R., Lanzani G., Mazzaro R., Corticelli F., Baroncini M., Barbarella G. Engineering thiophene-based nanoparticles to induce phototransduction in live cells under illumination. *Nanoscale*, **2017**, 9, 9202-9209.
9) Palamà I. E., Di Maria F., Zangoli M., D'Amone S., Manfredi G., Barsotti J., Lanzani G., Ortolani L., Salatelli E., Gigli G., Barbarella G. Enantiopure polythiophene nanoparticles. Chirality dependance of cellular uptake, intracellular distributionand antimicrobial activity. *RSC Adv*., **2019**, 9, 23036-23044.
10) Nezakati T., Seifalian A., Tan A., Seifalian A. M. Conductive Polymers: Opportunities and Challenges in Biomedical Applications. *Chem. Rev*., **2018**, 118, 6766-6843.
11) Di Maria F., Lodola F., Zucchetti E., Benfenati F., Lanzani G. The evolution of artificial light actuators in living systems: from planar to nanostructured interfaces. *Chem. Soc. Rev*., **2018**, 47, 13, 4757-4780.
12) Maya-Vetencourt J. F., Manfredi G., Mete M., Colombo E., Bramini M., Di Marco S., Shmal D., Mantero G., Dipalo M., Rocchi A., Di Francesco M. L., Papaleo E. D., Russo A., Barsotti J., Eleftheriou C., Di Maria F., Cossu V., Piazza F., Emionite L., Ticconi F., Marini C., Sambuceti G., Pertile G., Lanzani G., Benfenati F. Subretinally injected semiconducting polymer nanoparticles rescue vision in a rat model of retinal dystrophy. *Nat. Nanotechnol*., **2020**, 15, 698–708.
13) Francia S., Shmal D., Di Marco S., Chiaravalli G., Maya-Vetencourt J. F., Mantero G., Michetti C., Cupini S., Manfredi G., Di Francesco M. L., Rocchi A., Perotto S., Attanasio M., Sacco R., Bisti S., Mete M., Pertile G., Lanzani G., Colombo E., Benfenati F. Light-induced charge generation in polymeric nanoparticles restores vision in advanced-stage retinitis pigmentosa rats. *Nat. Commun.*, **2022**, 13, 3677.
14) Tortiglione C., Antognazza M. R., Tino A., Bossio C., Marchesano V., Bauduin A., Zangoli M., Vaquero Morata S., Lanzani G. Semiconducting polymers are light nanotransducers in eyeless animals. *Sci. Adv*., **2017**, 3, 1, e1601699.
15) Rand D., Jakešová M., Lubin G., Vėbraitė I., David-Pur M., Đerek V., Cramer T., Sariciftci N. S., Hanein Y., Głowacki E. D. Direct Electrical Neurostimulation with Organic Pigment Photocapacitors. *Adv. Mater.*, **2018**, 30, 1707292.
16) Fromherz P. Electrical Interfacing of Nerve Cells and Semiconductor Chips. *CHEMPHYSCHEM*, **2002**, 3, 276-284.
17) Schoen N., Fromherz P. The Mechanism of Extracellular Stimulation of Nerve Cells on an Electrolyte-Oxide-Semiconductor Capacitor. *Biophys J*., **2007**, 92, 1096-1111.
18) Doering C. J., McRory J. E. Effects of extracellular pH on neuronal calcium channel activation. *Neuroscience*, **2007**, 146, 3, 1032-1043.

19) Chiaravalli G., Manfredi G., Sacco R., Lanzani G. Photoelectrochemistry and Drift–Diffusion Simulations in a Polythiophene Film Interfaced with an Electrolyte. *ACS Appl. Mater. Interfaces.*, **2021**, 13, 30, 36595-36604.
20) Mosconi E., Salvatori P., Saba M. I., Mattoni A., Bellani S., Bruni F., Gonzalez B. S., Antognazza M. R., Brovelli S., Lanzani G., Li H., Brédas J.-L., De Angelis F. Surface Polarization Drives Photoinduced Charge Separation at the P3HT/Water Interface. *ACS Energy Lett*., **2016**, 1, 454-463.
21) Bellani S., Fazzi D., Bruno P., Giussani E., Canesi E. V., Lanzani G., Antogazza M. R. Reversible P3HT/Oxygen Charge Transfer Complex Identification in Thin Films Exposed to Direct Contact with Water. *J. Phys. Chem. C*, **2014**, 118, 6291-6299.
22) Zhuo J.-M., Zhao L.-H., Png R.-Q., Wong L.-W., Chia P.-J., Tang J.-C., Sivaramakrishnan S., Zhou M., Ou E. C.-W., Chua S.-J. Direct Spectroscopic Evidence for a Photodoping Mechanism in Polythiophene and Poly(bithiophene-*alt*-thienothiophene) Organic Semiconductor Thin Films Involving Oxygen and Sorbed Moisture. *Adv. Mater*., **2009**, 21, 4747-4752.
23) Bossio C., Abdel Aziz I., Tullii G., Zucchetti E., Debellis D., Zangoli M., Di Maria F., Lanzani G., Antognazza M. R. Photocatalytic Activity of Polymer Nanoparticles Modulates Intracellular Calcium Dynamics and Reactive Oxygen Species in HEK-293 Cells. *Front. Bioeng. Biotechnol*., **2018**, 6:114.
24) Di Maria F., Zanelli A., Liscio A., Kovtun A., Salatelli E., Mazzaro R., Morandi V., Bergamini G., Shaffer A., Rozen S. Poly(3-hexylthiophene) Nanoparticles Containing Thiophene-S,S-dioxide: Tuning of Dimensions, Optical and Redox Properties, and Charge Separation under Illumination. *ACS Nano*, **2017**, 11, 2, 1991-1999.
25) Zhang C., Wang X., Du J., Gu Z., Zhao Y. Reactive Oxygen Species-Regulating Strategies Based on Nanomaterials for Disease Treatment. *Adv. Sci*., **2021**, 8, 2002797.
26) Melitz W., Shen J., Kummel A.C., Lee S. Kelvin probe force microscopy and its application. *Surf. Sci. Rep.*, **2011**, 66, 1, 1-27.
27) Palermo V., Ridolfi G., Talarico A. M., Favaretto L., Barbarella G., Camaioni N., Samorì P. A Kelvin Probe Force Microscopy Study of the Photogeneration of Surface Charges in All-Thiophene Photovoltaic Blends. *Adv. Funct. Mater.*, **2007**, 17, 472-478.
28) Di Maria F., Zangoli M., Palamá I. E., Fabiano E., Zanelli A., Monari M., Perinot A., Caironi M., Maiorano V., Maggiore A., Pugliese M., Salatelli E., Gigli G., Viola I., Barbarella G. Improving the Property–Function Tuning Range of Thiophene Materials via Facile Synthesis of Oligo/Polythiophene-S-Oxides and Mixed Oligo/Polythiophene-S-Oxides/Oligo/Polythiophene-S,S-Dioxides. *Adv. Funct. Mater*., **2016**, 26, 6970-6984.
29) Liscio A., Palermo V., Müllen K., Samorì P. Tip−Sample Interactions in Kelvin Probe Force Microscopy: Quantitative Measurement of the Local Surface Potential. *J. Phys. Chem. C*, **2008**, 112, 44, 17368-17377.
30) He W., Liu Y., Wamer W. G., Yin J.-J. Electron spin resonance spectroscopy for the study of nanomaterial-mediated generation of reactive oxygen species. *J. Food Drug Anal.*, **2014**, 22, 49-63.
31) Dąbrowski J. M. Reactive Oxygen Species in Photodynamic Therapy: Mechanisms of Their Generation and Potentiation. *Adv. Inorg. Chem.*, **2017**, 70, 343-394.
32) An J., Tang S., Hong G., Chen W., Chen M., Song J., Li Z., Peng X., Song F., Zheng W.-H. An unexpected strategy to alleviate hypoxia limitation of photodynamic therapy by biotinylation of photosensitizers. *Nat. Commun.*, **2022**, 13, 2225.

33) Bielski B. H. J., Allen A. O. Mechanism of the disproportionation of superoxide radicals. *J. Phys. Chem.*, **1977**, 81, 11, 1048-1050.
34) Gilbert D. L., Colton C. A., **2002**, *Reactive Oxygen Species in Biological Systems*, Springer, Boston, MA.
35) Wu Y., Li S., Chen Y., He WGuo., Z. Recent advances in noble metal complex based photodynamic therapy. *Chem. Sci.*, **2022,** 13, 5085-5106.
36) Yamakoshi Y., Umezawa N., Ryu A., Arakane K., Miyata N., Goda Y., Masumizu T., Nagano T. Active Oxygen Species Generated from Photoexcited Fullerene (C_{60}) as Potential Medicines: $O_2^{-\bullet}$ versus $^1O_2$. *J. Am. Chem. Soc.*, **2003**, 125, 42, 12803-12809.
37) Dikalov S., Jiang J., Mason R. P. Characterization of the high-resolution ESR spectra of superoxide radical adducts of 5-(diethoxyphosphoryl)-5-methyl-1-pyrroline N-oxide (DEPMPO) and 5,5-dimethyl-1-pyrroline N-oxide (DMPO). Analysis of conformational Exchange. *Free Radic. Res.*, **2005**, 39, 8, 825-836.
38) Zhao H., Joseph J., Zhang H., Karoui H., Kalyanaraman B. Synthesis and biochemical applications of a solid cyclic nitrone spin trap: a relatively superior trap for detecting superoxide anions and glutathiyl radicals. *Free Radic. Biol. Med.*, **2001**, 31, 5, 599-606.
39) Wang H., Joseph J. A. Quantifying cellular oxidative stress by dichlorofluorescein assay using microplate reader. *Free Radic. Biol. Med.*, **1999**, 27, 612-616.
40) Bian Y., Guo J., Majeed H., Zhu K., Guo X., Peng W., Zhou H. Ferulic acid renders protection to HEK293 cells against oxidative damage and apoptosis induced by hydrogen peroxide. *In Vitro Cell Dev Biol Anim.*, **2015**, 51, 722-729.
41) Tortiglione C., Quarta A., Malvindi M. A., Tino A., Pellegrini T., *PLoS One*, **2009**. 4, e7698.
42) Ambrosone A., Tortiglione C., *Toxicol. Mech. Methods*, **2013**, 23, 207-216.
43) Allocca M., Mattera M., Bauduin A., Miedziak B., Moros M., De Trizio L., Tino A., Reiss P., Ambrosone A., Tortiglione C. Methodological approaches for nanotoxicology using cnidarian models. *Environ. Sci. Technol.*, **2019**, 53, 3938-3947.
44) Juan C. A., Pérez de la Lastra J. M., Plou F. J., Pérez-Lebeña E. The Chemistry of Reactive Oxygen Species (ROS) Revisited: Outlining Their Role in Biological Macromolecules (DNA, Lipids and Proteins) and Induced Pathologies. *Int J Mol Sci.*, **2021**, 22, 4642.
45) Valavanidis A., Vlachogianni T., Fiotakis C. 8-hydroxy-2' -deoxyguanosine (8-OHdG): A critical biomarker of oxidative stress and carcinogenesis. *J. Environ. Sci. Health. C Environ. Carcinog. Ecotoxicol. Rev.*, **2009**, 27, 120-39.
46) Moore L. D., Le T., Fan G. DNA Methylation and Its Basic Function. *Neuropsychopharmacol.*, **2013**, 38, 23-38.
47) Loomis W., Lenhoff H., *J. Exp. Zool.* Growth and sexual differentiation of hydra in mass culture. **1956**, 132, 555-574.
48) Moros M., Lewinska A., Onorato G., Antognazza M. R., Di Maria F., Blasio M., Lanzani G., Tino A., Wnuk M., Tortiglione C. Light-triggered modulation of cell antioxidant defense by polymer semiconducting nanoparticles in a model organism. *MRS Commun.*, **2018**, 8, 918-925.
49) Onorato G., Fardella F., Lewinska A., Gobbo F., Tommasini G., Wnuk M., Tino A., Moros M., Antognazza M. R., Tortiglione C. Optical Control of Tissue Regeneration Through Photostimulation of Organic Semiconducting Nanoparticles. *Adv. Healthc. Mater.*, **2022**, doi.org/10.1002/adhm.202200366.

GRAPHICAL ABSTRACT